RSC Advances

COMMUNICATION

View Article Online
View Journal | View Issue

Cite this: *RSC Adv.*, 2014, **4**, 32918

Received 1st June 2014
Accepted 16th July 2014

DOI: 10.1039/c4ra05199h

www.rsc.org/advances

A thin pristine non-triarylamine hole-transporting material layer for efficient $CH_3NH_3PbI_3$ perovskite solar cells

Junyan Xiao,[a] Liying Han,[b] Lifeng Zhu,[a] Songtao Lv,[a] Jiangjian Shi,[a] Huiyun Wei,[a] Yuzhuan Xu,[a] Juan Dong,[a] Xin Xu,[a] Yin Xiao,[b] Dongmei Li,*[a] Shirong Wang,[b] Yanhong Luo,[a] Xianggao Li*[b] and Qingbo Meng*[a]

A new non-traditional organic hole-transporting material (HTM), 4-(4-phenyl-4-α-naphthylbutadienyl)-*N*,*N*-bis(4-benzyl)-aniline (PNBA), has been employed in $CH_3NH_3PbI_3$ perovskite solar cells for the first time. The pore filling of PNBA into mesoporous TiO_2/$CH_3NH_3PbI_3$ scaffold is investigated in detail. As high as 11.4% of light-to-electricity conversion efficiency has been achieved, comparable to corresponding spiro-OMeTAD-based devices under the same conditions. It is revealed that the uniform and thin PNBA film is sufficient as a HTM for perovskite solar cells, and can facilitate hole transport to the metal cathode and also block electron transfer from the perovskite to the metal cathode.

Introduction

Organic–inorganic hybrid perovskite $CH_3NH_3PbI_3$ and its analogues have received remarkable attention due to their fascinating properties of suitable band gap, high extinction coefficient and long electron–hole diffusion length.[1,2] $CH_3NH_3PbX_3$ (X = Br, I) materials as sensitizers were first employed in sensitized solar cells in 2009 and were further optimized to 6.5% of power conversion efficiency, however, their chemical instability in the I_3^-/I^- liquid electrolyte makes the cell performance far from satisfactory.[3,4] Amazingly, the use of solid state hole-transporting materials (HTMs) has brought dramatic breakthroughs in the efficiency and stability of perovskite solar cells, and over 15% of power conversion efficiency has been achieved so far.[5,6] Very recently, perovskite solar cells without any HTM can also exhibit over 10% efficiency, still lower than HTM-based perovskite solar cells.[7] Generally, the existence of HTMs favours the hole transport to the Au electrode and blocks the electron transfer from perovskites to the Au electrode.

[a]*Key Laboratory for Renewable Energy (CAS), Beijing Key Laboratory for New Energy Materials and Devices, Beijing National Laboratory for Condense Matter Physics, Institute of Physics, Chinese Academy of Sciences, Beijing 100190, China. E-mail: qbmeng@iphy.ac.cn; dmli@iphy.ac.cn; Fax: +8610-82649242; Tel: +8610-82649242*

[b]*Co-Innovation Center of Chemistry and Chemical Engineering of Tianjin, School of Chemical Engineering and Technology, Tianjin University, Tianjin 300072, China*

Currently, three categories of HTMs are involved in this kind of thin film solar cell, including inorganic HTMs, polymeric HTMs and low molecular weight HTMs. Inorganic HTMs (*i.e.* CuI, CuSCN and NiO) were included in perovskite solar cells due to their high conductivity and the highest efficiency of 12.4% can be achieved, however, the disadvantages of restricted selection and deposition method will limit their further development.[8–12] On the contrary, organic HTMs including polymer HTMs and small molecular HTMs, display attractive diversity and can be modified by chemically tailored methods to fit different technological purposes. For example, polymer HTMs exhibit good stability and easy processing, and have been used in perovskite solar cells, such as poly(3-hexylthiophene) (P3HT), poly[2,1,3-benzothiadiazole-4,7-diyl[4,4-bis(2-ethylhexyl)-4*H*-cyclopenta[2,1-*b*:3,4-*b*′]dithiophene-2,6-diyl]] (PCPDTBT) and poly-triarylamine (PTAA), *etc.*[13] Over 12% efficiency was achieved for PTAA-based perovskite solar cells. In comparison with polymeric HTMs, low molecular weight HTMs are easier to control in terms of purification and modification, and are much easier to infiltrate into mesoporous photoanodes by a solution process. By using representative spiro-OMeTAD (2,2′,7,7′-tetrakis[*N*,*N*-di-*p*-methoxyphenylamine]-9,9′-spirobifluorene) as a low molecular weight HTM, perovskite solar cells can present over 15% efficiency regardless of whether mesoscopic Al_2O_3/TiO_2 scaffolds or planar heterojunction structures are involved. Recently, an impressively high efficiency of 16.7% was also achieved by utilizing the isomers of spiro-OMeTAD.[14] However, its price is too high to be of benefit for future commercialization.[15] Some efforts have been made to replace the spirobifluorene structure with other simple structures, such as pyrene and thiophene derivatives, which can present fairly good efficiency, however, the cost control of HTMs is still limited due to the relatively complicated synthetic process of triarylamine groups as well as the doping process.[16,17] As such, developing new HTMs with high efficiency and low cost is urgent for perovskite solar cells.

Herein, a new non-traditional triarylamine p-type small molecular hole-transporting material 4-(4-phenyl-4-α-naphthyl

butadienyl)-*N*,*N*-bis(4-benzyl)-aniline (PNBA) has been employed in $CH_3NH_3PbI_3$ perovskite solar cells. Its pore filling into mesoporous TiO_2 scaffold has been investigated detailedly, indicating that uniform and thin pristine PNBA film as the HTM is enough for the devices. A light-to-electricity conversion efficiency of 11.4% is achieved under AM 1.5 illumination (100 mW cm^{-2}), comparable to the perovskite solar cells with conventional spiro-OMeTAD under the same condition. Therefore, the existence of PNBA can facilitate the hole transport to metal cathode and block the electron transfer from the perovskite to the metal cathode as well. Advantages of cost effective, simple synthetic process and relatively high efficiency make the PNBA have the potential for the future application.

Results and discussion

The molecular structure of PNBA is shown in Fig. 1a, which is different from the general triarylamine structure. This makes its synthesis and purification processes easier and higher yield than those of PNBA's triarylamine derivative isomers, which are essential prerequisite to the future commercialization.[18] According to ultraviolet photoelectron spectroscopy (UPS) and cyclic voltammetry measurement, HOMO and LUMO energy levels of PNBA are determined to be −5.42 and −2.58 eV *vs.* vacuum level, respectively.[18] Obviously, PNBA exhibits suitable energy levels to smooth charge transport and charge collection in our $CH_3NH_3PbI_3$ perovskite solar cells, as shown in Fig. 1b.[19] Besides, its maximum absorption bands are located at 236, 275 and 380 nm, suggesting no strong influence on the light absorption of solar cells. The hole mobility of PNBA is 4.92×10^{-4} cm^2 V^{-1} s^{-1}, according to time-of-flight measurement.

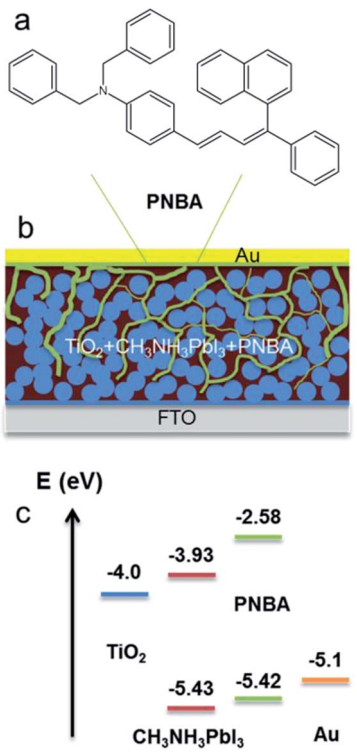

Fig. 1 (a) Molecular structure of PNBA; (b) scheme of the device structure; (c) energy levels of TiO_2/$CH_3NH_3PbI_3$/PNBA/Au in the device.

To perovskite solar cells with mesoporous scaffolds, the deposition of $CH_3NH_3PbI_3$ and HTMs is mainly based on spin coating technique, which unavoidably has a high correlation with the infiltration depth and the filling fraction (*i.e.* volume fraction of the pores filled by HTMs). In our systems, due to the same TiO_2 film and spin coating condition for $CH_3NH_3PbI_3$ deposition, it is thus considered that light absorbance and electron injection efficiency ($\eta_{e\text{-}inj}$) are identical for $CH_3NH_3PbI_3$ solar cells with different thickness PNBA films. Moreover, the cell performance is also strongly dependent on the hole injection efficiency ($\eta_{h\text{-}inj}$), which is directly influenced by PFF of HTMs. Currently, only a few work about the HTM filling have been reported in perovskite solar cells.[20–23] Here, the PNBA filling into the mesoscopic scaffold is firstly investigated. In order to understand the pore-filling-fraction (PFF) of PNBA in the mesoporous TiO_2/perovskite film, a simplified sample of PbI_2-coated TiO_2 porous film with 400 nm thickness (PbI_2/TiO_2/PNBA) is adopted. According to Snaith's work about the pore-filling and solvent evaporation processes in fabricating solid-state dye-sensitized solar cells,[24] an approximate formula for our system is suggested as follows:

$$\mathrm{PFF} = c + (c \times t_{\mathrm{wet}} - t_{\mathrm{OL}})/(t_{\mathrm{TiO_2}} \times p) \quad (1)$$

where PFF is the pore-filling-fraction, c is the volume ratio of PbI_2 or PNBA in solution, t_{wet} is the wet reservoir thickness in spin-coating process, t_{OL} is the PbI_2 or PNBA overlayer thickness, t_{TiO_2} is the TiO_2 film thickness, and p is the film porosity. According to this formula, it can be inferred that the value of PFF is mainly determined by $c/(t_{TiO_2} \times p)$.

UV-vis absorption spectroscopy is employed to estimate the PFFs of PbI_2 and PNBA, respectively.[25] The detailed experimental process is as follows: the PbI_2 and PNBA (20 mg mL^{-1} in chlorobenzene) are successively spin-coated on 2.0 cm^2 TiO_2 to give the PNBA/PbI_2/TiO_2 film, which is re-dissolved firstly in 2 mL chlorobenzene to give the PNBA solution, then in 2 mL DMF to give the PbI_2 solution. According to the absorption spectra of PbI_2 and PNBA (see Fig. 2), the total mass of PbI_2 and PNBA are 0.199 mg and 0.022 mg. It thus the porosity of TiO_2 film decreases from 65% to 33% after PbI_2 (6.16 g cm^{-3}) deposition, and further to 14% after PNBA filling (1.15 g cm^{-3}, calculated with ChemSketch software). Therefore, a PFF value of 57% is estimated after PNBA is deposition on PbI_2/TiO_2 film. Under the same experimental condition, the PFF value is estimated to be 54% for the spiro-OMeTAD/PbI_2/TiO_2 film. In fact, after soaking in CH_3NH_3I solution (10 mg mL^{-1}), the PbI_2 in porous TiO_2 film will convert into $CH_3NH_3PbI_3$ while the volume increasing, which is supposed to lead to smaller p value and a higher PFF value.[26] Considering the volume of PNBA molecule is much smaller than that of spiro-OMeTAD (1.6×10^{-27} *vs.* 3.0×10^{-27} m^3, calculated with QSAR method), the former may be easier to infiltrate and finally achieve a higher PFF value. Therefore, it is suggested that the PNBA solution with the concentration of 20 mg mL^{-1} be sufficient to achieve effective pore-filling to perovskite solar cells.

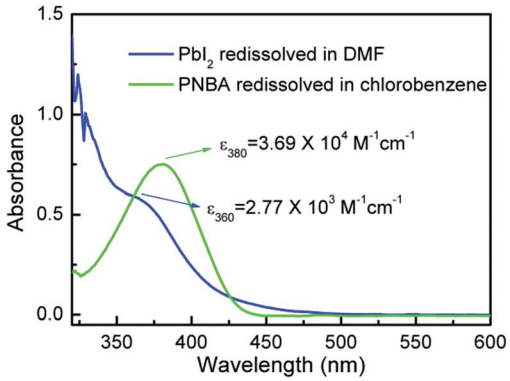

Fig. 2 UV-vis absorption spectra of re-dissolved PbI_2 and PNBA in DMF and chlorobenzene solution from a simplified device sample.

Under low *c* value (1.7% for 20 mg mL^{-1} PNBA) and sufficient PFF value, the thickness of HTM overlayer may be very thin, which can be convinced by SEM images in Fig. 3. Fig. 3a exhibits the top view image of $CH_3NH_3PbI_3/TiO_2$ film. As can be seen, a porous structure decorated by $CH_3NH_3PbI_3$ with diameters of about 100 nm is observed on the top of the TiO_2 film. After spin-coating with 20 mg mL^{-1} PNBA chlorobenzene solution, the top morphology of PNBA/$CH_3NH_3PbI_3/TiO_2$ film is almost unchanged except for a little indistinct on the surface and some pores partially filled, indicating a thin HTM layer exists on the surface of the $CH_3NH_3PbI_3/TiO_2$ film, as shown in Fig. 3b. The cross-sectional SEM image of this PNBA/$CH_3NH_3PbI_3/TiO_2$ sample is also exhibited in Fig. 3c, in which the PNBA layer can hardly be observed. And in contrast, the $CH_3NH_3PbI_3/TiO_2$ film is covered with an apparent thick PNBA layer in the sample fabricated with 20 mg mL^{-1} PNBA, as shown in Fig. 3d.

Perovskite solar cells with $CH_3NH_3PbI_3/TiO_2$/PNBA/Au structure were fabricated by a sequential deposition method.[6,27] Under standard AM 1.5 illumination (100 mW cm^{-2}), the device exhibits short-circuit photocurrent density (J_{sc}) of 17.5 mA cm^{-2}, open-circuit photovoltage (V_{oc}) of 0.945 V, fill factor (FF) of 0.689, yielding the light-to-electricity conversion efficiency (η) of 11.4%, as shown in Fig. 4a. Furthermore, the IPCE spectra of $CH_3NH_3PbI_3$ perovskite sensitized solar cell with 20 mg mL^{-1} PNBA is presented. As can be seen in Fig. 4b, the IPCE value at the wavelength of 500 nm is 85%, which incident light loss is supposed to be caused by front reflection. And the integral current value (16.5 mA cm^{-2}) calculated from IPCE spectra is in good agreement with the experimental J_{sc}. Obviously, the separation and injection processes of photo-generated carriers in the device are effective under the low light intensity irradiation during IPCE measurement.[28] It is thus suggested that the HOMO energy level of PNBA is suitable for the $CH_3NH_3PbI_3/TiO_2$/PNBA/Au system.

To further clarify the influence of pore filling of PNBA on the cell performance, different PNBA concentrations with 2 and 80 mg mL^{-1} PNBA in chlorobenzene have also been used to fabricate the devices. Their photovoltaic characteristics are exhibited as Fig. 5, and the parameters are summarized in Table 1. As can be seen, the device fabricated with 2 mg mL^{-1} PNBA shows the short-circuit photocurrent density (J_{sc}) of 15.3 mA cm^{-2}, open-circuit photovoltage V_{oc} of 890 mV and fill factor (FF) of 0.604, yielding the power conversion efficiency (PCE) of 8.2%. It is thus supposed that under such a low PNBA concentration, the top surface of $CH_3NH_3PbI_3$ layer is coated with an ultrathin PNBA layer, but the PFF (estimated to 9%) may be insufficient. This difference on PFF will lead to the decrease in all the four parameters (J_{sc}, V_{oc}, FF and PCE), which is in agreement with the phenomena observed in solid-state dye-

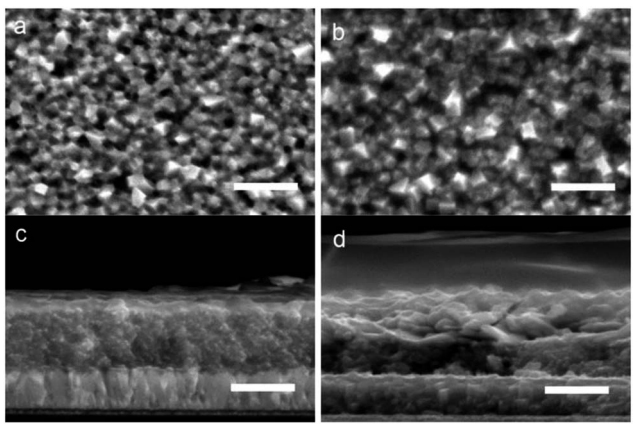

Fig. 3 Top view SEM images of (a) bare $CH_3NH_3PbI_3/TiO_2$ film and (b) $CH_3NH_3PbI_3/TiO_2$/PNBA film; cross-sectional SEM images of $CH_3NH_3PbI_3/TiO_2$ film covered with (c) 20 mg mL^{-1} PBNA and (d) 80 mg mL^{-1} PBNA. The scale bars in images are 500 nm.

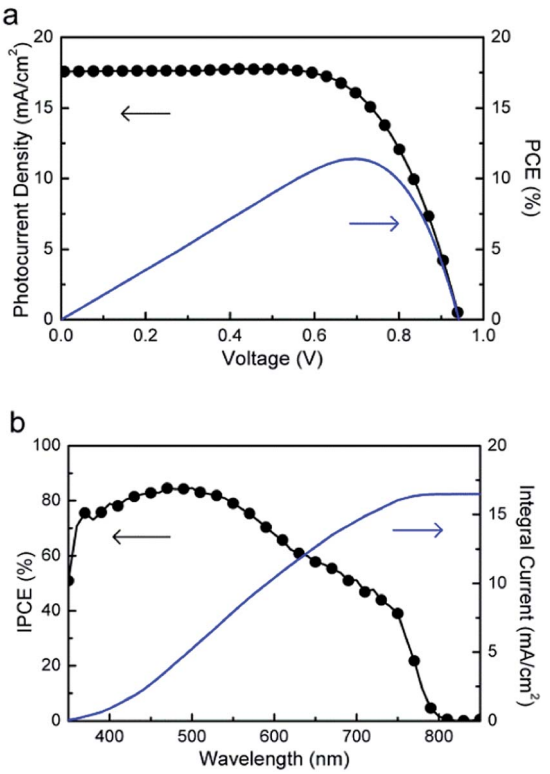

Fig. 4 (a) *J*–*V* characteristics and (b) IPCE spectra of perovskite solar cell with 20 mg mL^{-1} PNBA.

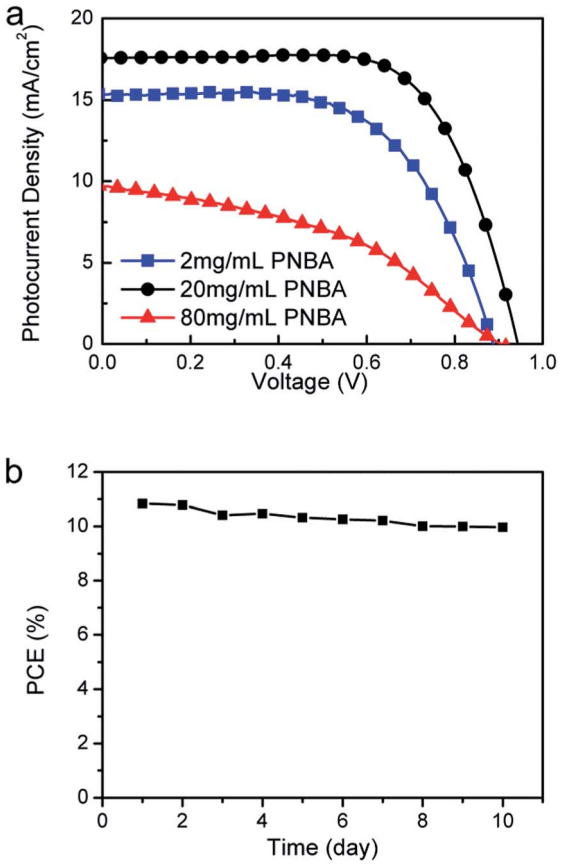

Fig. 5 (a) *J–V* characteristics of perovskite solar cells with different PNBA solution concentrations; (b) evolution of average photovoltaic parameters of six unsealed cells. During the stability test, the cells were kept at temperature around 25 °C with humidity of 30% under dark condition.

Table 1 Parameters of photovoltaic performances of perovskite solar cells with different HTM concentrations

Device	J_{sc} mA cm^{-2}	V_{oc} V	FF	PCE %	R_s Ω cm^{-2}
2 mg mL^{-1}	15.3	0.890	0.604	8.2	10.2
20 mg mL^{-1}	17.5	0.945	0.689	11.4	8.6
80 mg mL^{-1}	9.7	0.900	0.421	3.7	64.0

sensitized solar cells.[29] Besides, the cell performance of the device utilizing 80 mg mL^{-1} PNBA solution is still poor, as shown in Table 1. Considering this device is effectively filled with PNBA but has a thick HTM overlayer on the top surface as shown in Fig. 3d, the poor performance is mainly due to the thick pristine HTM overlayer, which introduces large series resistance to the device. In comparison, the perovskite solar cells with the same concentration of pristine spiro-OMeTAD doped with LiTFSI and 4-*tert*butylpyridine in chlorobenzene were also fabricated, which can present similar cell performance with the J_{sc} of 18.7 mA cm^{-2}, V_{oc} of 973 mV, FF of 0.714 and PCE of 13.0%.[6] In fact, since $CH_3NH_3PbI_3$ itself is also the hole conductor, it is thus suggested that when the $CH_3NH_3PbI_3$ film morphology can be well controlled, such as the complete filling of TiO_2 pores by $CH_3NH_3PbI_3$ to give the smooth and uniform surface, much lower PNBA concentrations (*i.e.* 2 mg mL^{-1}) or even HTM-free may also make the cells work efficiently.

Obviously, this ultrathin pristine HTM layer strategy can also prevent high series resistance. Together with efficient PNBA pore-filling, this HTM structure in perovskite solar cell can afford good photovoltaic performance. Furthermore, six unsealed cells were tested every day and kept in ambient atmosphere to investigate their stability. After 10 days, the average efficiency retained 90% of the initial value, as shown in Fig. 5b.

Experimental section

Materials

PbI_2 was purchased from Aldrich, *N*,*N*-dimethylformamide (DMF) and chlorobenzene from Alfar Aesar. All the chemicals were directly used without further purification. CH_3NH_3I was synthesized by following the literature.[5] Substrates are fluorine-doped tin oxide conducting glass (FTO, Pilkington, thickness: 2.2 mm, sheet resistance 14 Ω per square). Before use, FTO glass was firstly washed with mild detergent, rinsed with distilled water for several times and subsequently with ethanol in an ultrasonic bath, finally dried under air stream. 4-(4-phenyl-4-α-naphthylbutadienyl)-*N*,*N*-bis(4-benzyl)-aniline (PNBA), which molecular structure is shown in Fig. 1a, was prepared according to our previous work.[18] Some characterizations of PNBA compound are as follows: Mp = 148–149.5 °C, IR (cm^{-1}, KBr): 3020, 2897, 1598, 1509, 1353, 958, 731, 697. ^{1}H NMR (500 MHz $CDCl_3$) δ (ppm): 4.606 (s, 4H), 6.636–6.667 (d, 1H, J = 15.5), 6.549–6.564 (d, 2H, J = 7.5), 6.980–6.998 (d, 2H, J = 9.0), 7.173–7.456 (m, 19H), 7.521–7.5551 (t, 1H), 7.714–7.731 (d, 2H, J = 8.5), 7.780–7.896 (d, 2H, J = 5.8). MS (*m*/*z*): 527.27 (calcd) and 528.27 (found) for $[M + 1]^+$.

Device fabrication

50 nm-thickness TiO_2 compact layer and 500 nm-thickness mesoporous TiO_2 anatase layer were deposited on FTO glass in sequence by screen printing method according to the literature.[7] Then, $CH_3NH_3PbI_3$ was deposited on TiO_2 porous films according to a sequential deposition method.[6] That is, 1.2 M PbI_2 in DMF was spin-coated on the TiO_2 film at 3000 rpm for 60 s, then heated at 90 °C for 2 min, finally soaked into CH_3NH_3I isopropanol solution (10 mg mL^{-1}) for 10 min. The film color changes from yellow to dark brown. The obtained $CH_3NH_3PbI_3$/TiO_2 films were thoroughly rinsed with isopropanol, dried under air stream, finally heated at 90 °C for 45 min in air on a hotplate. PNBA was further deposited on $CH_3NH_3PbI_3$/TiO_2 films by spin coating at 3000 rpm with PNBA chlorobenzene solutions. Finally, 80 nm of gold was thermally evaporated on top of the PNBA layer as counter electrode.

Characterization

Film thicknesses were determined by a surface profiler (KLA-Tencor). The morphologies of the films were obtained with scanning electron microscopy (SEM, FEI, XL30 S-FEG). UV-vis absorption spectra of the PbI_2 in DMF and PNBA in chlorobenzene were obtained on UV-2550 spectrophotometer, Shimadzu. The cells were illuminated under 100 mW cm^{-2} (AM 1.5) on Oriel Solar Simulator 91192. Photocurrent density–photovoltage (*J–V*) characteristics of the devices were recorded on Princeton Applied Research Model 263A. Incident-photon-to-current conversion efficiency (IPCE) was carried out by direct current (DC) method using a lab-made IPCE setup.[28] The time-of-flight (TOF) measurement was carried out on TOF401 (Sumitomo Heavy Industries. Ltd, Japan). The sample was prepared by vacuum deposition using a structure ITO/HTM (about 1 μm)/Al (150 nm) having an active area of 3×10 mm^2. Infrared absorption spectra were measured with Thermo Nicolet 380, Thermo.^{1}H NMR spectra were carried out on INOVA 500 MHz, Varian. Mass spectrometry was determined by FINNIGAN LCQ Advantage, Finnigan.

Conclusions

In summary, a novel pristine non-triarylamine HTM has been employed in $CH_3NH_3PbI_3$ perovskite solar cells. The PFF of HTM in mesoscopic scaffolds is determined to be sufficient by both theoretical and experimental methods. Because of the effective filling, the device with ultrathin overlayer structure of PNBA exhibits a high PCE of 11.4%, comparable to the performances of spiro-OMeTAD and other triarylamine-based HTM.[30] This result may provide a new way to further optimize the HTM-based perovskite solar cells. Furthermore, the PNBA as HTM in this work is low-cost, which can avoid the complicated synthesis of triarylamine derivatives and significantly reduce the cost of devices.

Acknowledgements

The authors would like to thank the financial support from Beijing Science and Technology Committee (no. Z131100006013003), the MOST (973 projects, nos. 2012CB932903 and 2012CB932904, 863 project, no. 2012AA030307), NSFCs (nos. 51372270, 51372272 and 21173260) and the Knowledge Innovation Program of the Chinese Academy of Sciences.

Notes and references

1 G. Xing, N. Mathews, S. Sun, S. S. Lim, Y. M. Lam, M. Grätzel, S. Mhaisalkar and T. C. Sum, *Science*, 2013, **342**, 344.
2 S. D. Stranks, G. E. Eperon, G. Grancini, C. Menelaou, M. J. P. Alcocer, T. Leijtens, L. M. Herz1, A. Petrozza and H. J. Snaith, *Science*, 2013, **342**, 341.
3 A. Kojima, K. Teshima, Y. Shirai and T. Miyasaka, *J. Am. Chem. Soc.*, 2009, **131**, 6050.
4 J. Im, C. Lee, J. Lee, S. Park and N. Park, *Nanoscale*, 2011, **3**, 4088.
5 H. Kim, C. Lee, J. Im, K. Lee, T. Moehl, A. Marchioro, S. Moon, R. Humphry-Baker, J. Yum, J. E. Moser, M. Grätzel and N. Park, *Sci. Rep.*, 2012, **2**, 591.
6 J. Burschka, N. Pellet, S. Moon, R. Humphry-Baker, P. Gao, M. K. Nazeeruddin and M. Grätzel, *Nature*, 2013, **499**, 316.
7 J. Shi, J. Dong, S. Lv, Y. Xu, L. Zhu, J. Xiao, X. Xu, H. Wu, D. Li, Y. Luo and Q. Meng, *Appl. Phys. Lett.*, 2014, **104**, 063901.
8 J. A. Christians, R. C. M. Fung and P. V. Kamat, *J. Am. Chem. Soc.*, 2014, **136**, 758.
9 S. Ito, S. Tanaka, H. Vahlman, H. Nishino, K. Manabe and P. Lund, *ChemPhysChem*, 2014, **15**, 1194.
10 S. Chavhan, O. Miguel, H. Grande, V. Gonzalez-Pedro, R. S. Sánchez, E. M. Barea, I. Mora-Seró and R. Tena-Zaera, *J. Mater. Chem. A*, 2014, DOI: 10.1039/C4TA01310G.
11 P. Qin, S. Tanaka, S. Ito, N. Tetreault, K. Manabe, H. Nishino, M. K. Nazeeruddin and M. Grätzel, *Nat. Commun.*, 2014, **5**, 3834.
12 K. Wang, J. Jeng, P. Shen, Y. Chang, E. W. Diau, C. Tsai, T. Chao, H. Hsu, P. Lin, P. Chen, T. Guo and T. Wen, *Sci. Rep.*, 2014, **4**, 4756.
13 J. H. Heo, S. H. Im, J. H. Noh, T. N. Mandal, C. Lim, J. A. Chang, Y. H. Lee, H. Kim, A. Sarkar, M. K. Nazeeruddin, M. Grätzel and S. I. Seok, *Nat. Photonics*, 2013, **7**, 486.
14 N. J. Jeon, H. G. Lee, Y. C. Kim, J. Seo, J. H. Noh, J. Lee and S. I. Seok, *J. Am. Chem. Soc.*, 2014, **136**, 7837.
15 U. Bach, D. Lupo, P. Comte, J. E. Moser, F. Weissörtel, J. Salbeck, H. Spreitzer and M. Grätzel, *Nature*, 1998, **395**, 583.
16 N. J. Jeon, J. Lee, J. H. Noh, M. K. Nazeeruddin, M. Grätzel and S. I. Seok, *J. Am. Chem. Soc.*, 2013, **135**, 19087.
17 T. Krishnamoorthy, F. Kunwu, P. P. Boix, H. Li, T. M. Koh, W. L. Leong, S. Powar, A. Grimsdale, M. Grätzel, N. Mathews and S. G. Mhaisalkar, *J. Mater. Chem. A*, 2014, **2**, 6305.
18 L. Y. Han, Master thesis, Tianjin University, 2013.
19 R. Lindblad, D. Bi, B. Park, J. Oscarsson, M. Gorgoi, H. Siegbahn, M. Odelius, E. M. J. Johansson and H. Rensmo, *J. Phys. Chem. Lett.*, 2014, **5**, 648.
20 T. Leijtens, G. E. Eperon, S. Pathak, A. Abate, M. M. Lee and H. J. Snaith, *Nat. Commun.*, 2013, **4**, 2885.
21 A. Dualeh, T. Moehl, N. Tétreault, J. Teuscher, P. Gao, M. K. Nazeeruddin and M. Grätzel, *ACS Nano*, 2014, **8**, 362.
22 H. Kim, J. Lee, N. Yantara, P. P. Boix, S. A. Kulkarni, S. Mhaisalkar, M. Grätzel and N. Park, *Nano Lett.*, 2013, **13**, 2412.
23 T. Leijtens, B. Lauber, G. E. Eperon, S. D. Stranks and H. J. Snaith, *J. Phys. Chem. Lett.*, 2014, **5**, 1096.
24 H. J. Snaith, R. Humphry-Baker, P. Chen, I. Cesar, S. M. Zakeeruddin and M. Grätzel, *Nanotechnology*, 2008, **19**, 424003.
25 I. Ding, N. Tétreault, J. Brillet, B. E. Hardin, E. H. Smith, S. J. Rosenthal, F. Sauvage, M. Grätzel and M. D. McGehee, *Adv. Funct. Mater.*, 2009, **19**, 2431.

26 T. Baikie, Y. Fang, J. M. Kadro, M. Schreyer, F. Wei, S. G. Mhaisalkar, M. Grätzel and T. J. White, *J. Mater. Chem. A*, 2013, **1**, 5628.
27 D. Bi, S. J. Moon, L. Häggman, G. Boschloo, L. Yang, E. M. J. Johansson, M. K. Nazeeruddin, M. Grätzel and A. Hagfeldt, *RSC Adv.*, 2013, **3**, 18762.
28 X. Guo, Y. Luo, Y. Zhang, X. Huang, D. Li and Q. Meng, *Rev. Sci. Instrum.*, 2010, **81**, 103106.
29 J. Melas-Kyriazi, I. Ding, A. Marchioro, A. Punzi, B. E. Hardin, G. F. Burkhard, N. Tétreault, M. Grätzel, J. E. Moser and M. D. McGehee, *Adv. Energy Mater.*, 2011, **1**, 407.
30 J. Wang, S. Wang, X. Li, L. Zhu, Q. Meng, Y. Xiao and D. Li, *Chem. Commun.*, 2014, **50**, 5829.